Suppressed hydrogen chemisorption of zeolite encaged metal clusters: discrimination between theoretical models on the basis of Ru/NaY

Timothy J. McCarthy, Clélia M.P. Marques, Horacio Treviño and Wolfgang M.H. Sachtler*

V.N. Ipatieff Laboratory, Center for Catalysis and Surface Science, Department of Chemistry, Northwestern University, Evanston, IL 60208, USA

Received 28 August 1996; accepted 7 November 1996

The effects of thermal treatment and zeolite proton concentration on the chemical state and metal particle size of zeolite Y supported ruthenium (3.0 wt%) have been investigated using H_2-TPR, H_2-TPD, TPMS, FTIR, TEM, and EXAFS. Heating in Ar of the precursor after ion exchange, $[Ru(NH_3)_6]^{3+}$/NaY, up to 400°C leads to nearly 100% *autoreduction* of the ruthenium, as evidenced by H_2-TPR and TPMS. Heating in O_2 results in the formation of volatile ruthenium oxides. After autoreduction, the Ru clusters are extremely small, their coordination numbers, derived from EXAFS, are 0.6 for Ru/HY and 0.8 for Ru/NaY. Subsequent treatment at 500°C in flowing H_2 induces Ru agglomeration to particles which are about the size of the zeolite Y supercages, as indicated by TEM and EXAFS. The Ru–Ru distances are contracted compared to bulk Ru metal. Washing of autoreduced Ru/NaY with NaOH, thus removing the protons formed during autoreduction, results in Ru agglomeration to large particles (60–100 Å). Comparison of the hydrogen adsorption of Ru clusters with similar sizes of 10–15 Å reveals a marked interaction of the Ru clusters with zeolite protons. Increasing the H^+/Ru ratio from 3 for Ru/NaY to 10 for Ru/HY, results in a suppression of hydrogen chemisorption per Ru atom by 75%. The conclusion that formation of metal–proton adducts affects the electronic structure of the Ru clusters, thus being one of the main causes of the lowering of the heat of hydrogen chemisorption, is supported by FTIR data of adsorbed CO. The most pronounced C–O vibration band in Ru/HY is located at 2099 cm^{-1}; this band is absent in Ru/NaY. Significant blue-shifting of the IR bands is in conformity with *electron-deficiency* of the Ru clusters in Ru/HY. The results confirm that adsorptive properties of zeolite encaged metal clusters can be "tuned" by other ions sharing the same cavities.

Keywords: ruthenium in zeolite-Y, electron-deficiency, H_2 chemisorption on nanoclusters

1. Introduction

It has been shown for transition metal/zeolite Y systems (Pt, Pd, Rh) that anchoring of metal particles via metal–proton adducts leads to very small metal clusters (< 10 Å) and an unusual suppression of their propensity to adsorb hydrogen [1,2]. While it is conceivable that dissociative chemisorption of H_2 will be less facile on isolated metal atoms than on their clusters [3], it is less clear why the true metal dispersion of very small clusters deviates so strongly from the measured ratio of $H_{adsorbed}/M$. Two possible causes had been considered for this suppression of the hydrogen chemisorption by some clusters:

(1) Small metal clusters have non-metallic, discrete energy levels. In this view the small size of the clusters is the main cause for the suppressed hydrogen adsorption.

(2) Interaction of the clusters with zeolitic protons lowers the heat of hydrogen adsorption. Recently, density function calculations have been shown to support the metal–proton adduct model for the Pd/zeoliteY and Pt/mordenite systems [4,5].

In previous research with zeolite supported metal clusters, it appeared impossible to discriminate between these hypotheses, because extremely high metal dispersion always required presence of zeolite protons. The objective of the present paper is to clarify the issue of suppressed hydrogen chemisorption by separating the variables of metal particle size and zeolite proton/metal interaction in the system ruthenium/zeolite Y. For this combination it has been suggested, by Wang et al., that suppression of H_2 adsorption is due to the interaction of the zeolite protons with ruthenium metal particles [6].

2. Experimental

2.1. Catalyst preparation and pretreatment

The NaY and NH_4Y zeolite supports were prepared from LZ Y-52 (Si/Al = 2.6, Linde Molecular Sieves, Lot No. 968087061020-S-8). Two successive exchanges with a 20 molar excess of $NaNO_3$ at room temperature were performed to yield NaY. NH_4Y (90% exchange) was prepared by three successive exchanges having a 10 molar excess of NH_4Cl (solution temperature = 80°C).

Ruthenium was ion-exchanged into the support to achieve a weight loading of 3% Ru/NaY and 3% Ru/

* To whom correspondence should be addressed.

NH_4Y. A typical procedure involved slowly adding a dilute solution of $[Ru(NH_3)_6]Cl_3$ (Johnson Matthey) (0.002 M) to a rapidly stirred zeolite slurry (3 g/ℓ) at room temperature over a 8 h period, followed by additional stirring for 16 h. After drying in air at room temperature, the metal loading was determined by ICP elemental analysis.

Neutralization of the protons formed during the reduction of Ru ions in the Ru/NaY sample was performed to give Ru^N/NaY. The protons in the reduced catalyst were back-exchanged with two successive treatments with a 1 M aqueous solution of $NaNO_3$ at room temperature. Neutralization with a NaOH solution was also attempted. A NaOH solution was added dropwise to a stirring slurry of Ru/NaY in water and the pH was adjusted to 9.5.

Pretreatments for the Ru catalysts were carried out in a helium flow (High Purity, Linde, 60 ml/min) while the temperature was ramped at 2°C/min to 400°C, then held at the respective temperature for 20 min. A faster heating rate of 6°C/min to 400°C in helium was implemented as a dehydration step prior to reduction for the Ru^N/NaY samples. Heating in helium was necessary to avoid the formation of volatile RuO_4 [7]. The helium and hydrogen were purified by passing them over MnO/SiO_2 and a 4A molecular sieve.

Prior to reaction, all samples were heated to 500°C in H_2 (UHP, Linde, 30 ml/min) at 8°C/min and then held at that temperature for 20 min. The samples were then cooled to the reaction temperature under H_2, then switched to He prior to reaction.

2.2. Fourier transform infrared spectroscopy (FTIR)

A Nicolet 60 SX FTIR spectrometer operating at 1 cm^{-1} resolution was used for all analyses. Samples were pressed into thin, self-supporting wafers and placed in a quartz IR cell designed for in situ pretreatment. Following a thermal treatment in Ar (400°C), samples were reduced in H_2 at 30 ml/min using the thermal profile: 20 to 450°C at 6°C/min followed by a 30 min temperature hold. After reduction, the IR cell was purged with a flow of He (50 ml/min) for 15 min and then the spectra were recorded. For those experiments involving analysis of ruthenium carbonyl species, the catalysts were exposed to a flow of CO (30 ml/min) for 5 min at 20°C. The cell was then purged for 15 min in He (50 ml/min) and the spectra were recorded.

2.3. Temperature-programmed reduction (TPR) and desorption (TPD)

Following a thermal treatment in Ar to 400°C, samples were cooled to −80°C in a flow of Ar (60 ml/min). The gas was then switched to 5% H_2/Ar (25 ml/min) and the TPR commenced. The thermal time profile was as follows: −80 to 500°C at 8°C/min followed by a 20 min temperature hold. The H_2 consumption was monitored with a thermal conductivity detector (TCD) connected to a PC data station. Following reduction, samples were cooled to 20°C in Ar. They were exposed to 5% H_2/Ar for 30 min followed by a 15 min purge in Ar at 25 ml/min. The system was then cooled to −80°C for the start of the TPD. The temperature profile of the TPD experiments was identical to the one used in the TPR experiments. Errors in the quantification of the TPR and TPD experiments are determined to be ±5% and ±10%, respectively.

2.4. Temperature-programmed mass-spectrometric analysis (TPMS)

TPMS was employed to probe the decomposition products of the $Ru(NH_3)_6^{3+}$ complexes in the samples. The catalyst (300 mg) was heated in a packed-bed reactor under Ar (30 ml/min) from 20 to 500°C at 8°C/min and held at 500°C for 20 min. Data were recorded using a Dycor M200 quadrupole mass analyzer (Ametek). The data obtained represent the integral production of mass 15, which is due to the fragmentation of NH_3. The masses for H_2 (2), H_2O (18) and N_2 (28) were also monitored.

2.5. Transmission electron microscopy (TEM)

A Hitachi HF-2000 high-resolution analytical electron microscope equipped with a field emission cathode was used for ruthenium particle size analysis. The microscope was operated at 200 keV in the bright field mode. The ex situ treated catalysts were supported on holey carbon coated copper grids for the experiment. The microscope was also equipped with an Oxford Link QX2000 EDS elemental analysis probe.

2.6. Extended X-ray absorption fine structure (EXAFS)

Ru K-edge (22.117 keV) EXAFS data were collected in the transmission mode at −185°C at the B2 station of the Cornell High Energy Synchrotron Source (CHESS) (Ithaca, NY). The samples were pressed into pellets, mounted into the cell and heated in He to 400°C and reduced in situ at a temperature of 500°C in a 20 ml/min flow of 5% H_2/He. The cell used in the studies was constructed of stainless steel and equipped with kapton film windows. The EXAFS data analysis was based on experimentally determined phase shifts and backscattering amplitudes of a structure standard, ruthenium black (Aldrich) and ruthenium dioxide (Aldrich). The coordination number (CN) of Ru in the standard was taken as 12 with a nearest neighbor bond distance, R_{Ru-Ru}, of 0.267 nm. The data were analyzed with BAN (vol. 4.48), a PC-based EXAFS analysis program obtained from Tolmar Instruments (Hamilton, Canada).

3. Results

3.1. TPMS

The TPMS data for Ru/NH_4Y and Ru/NaY are shown in fig. 1. The results show two main N_2 evolution peaks at 350 and 420°C. Ammine decomposition and subsequent autoreduction begins at ~ 300°C and is not complete until > 400°C. Evolution of N_2 and H_2 are observed at ~ 420°C. A second TPMS experiment performed with Ru/HY after pretreatment in argon at 400°C confirmed that there was no additional ammine and ammonium ion decomposition.

3.2. TPR-TPD

After pretreatment of Ru/NaY or Ru/NH_4Y to 400°C under argon, 100% autoreduction was confirmed by TPR. Additional TPR's were performed to 650°C in order to rule out the presence of Ru^{3+}, which could be located in sodalite cages or hexagonal prisms. After back-exchange of Ru/NaY with $NaNO_3$ in air at room temperature, TPR shows an oxide peak centered at 75°C (fig. 2), which gives a H/Ru_{total} ratio of 3.51. The TPD data are shown in table 1 and are expressed as H/Ru_{total} molar ratios. For samples that were autoreduced only, a second high-temperature TPD peak at > 400°C was observed. An exceptionally low value for Ru/HY is noteworthy.

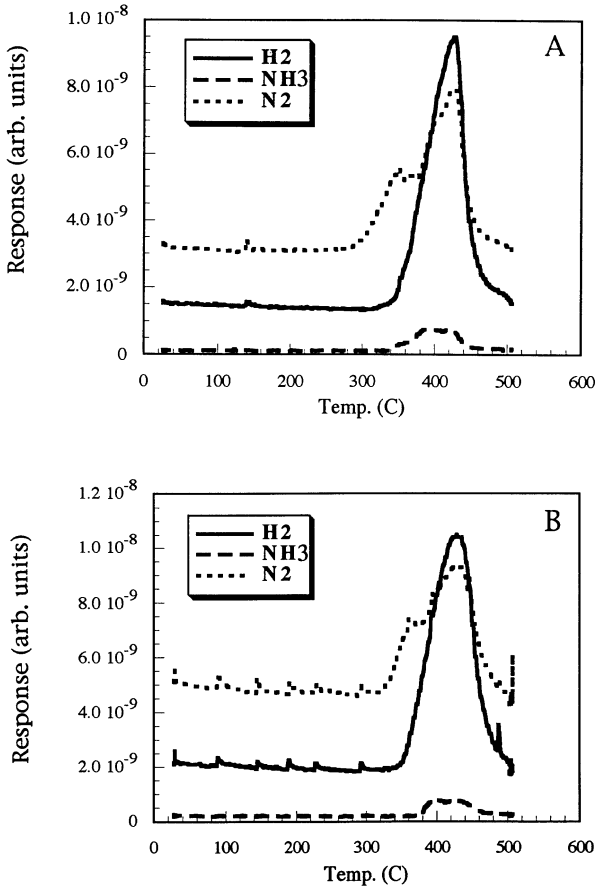

Fig. 1. TPMS profiles of: (A) Ru/NaY and (B) Ru/NH_4Y.

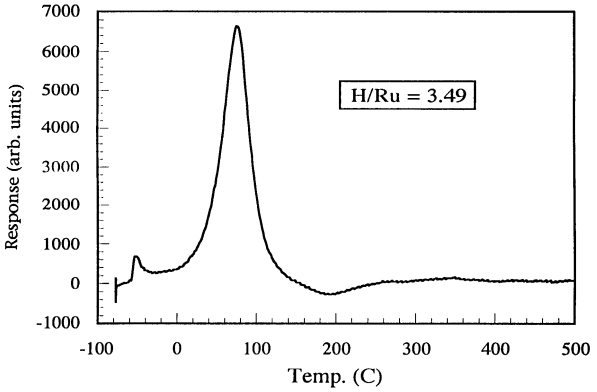

Fig. 2. TPR profile of Ru^N/NaY after neutralization.

3.3. FTIR

Fig. 3 shows the IR spectra in the CO region (1900–2300 cm^{-1}) for (A) Ru/NaY and (B) Ru/HY after addition of CO. There was no evidence of bridging CO bands below 1900 cm^{-1}. The purpose of the experiment was to determine if the presence of protons leads to a shift to higher energy due to electron deficiency on the Ru metal clusters. There are two regions of interest in the CO spectra of Ru/HY and Ru/NaY. A high energy region (2128–2159 cm^{-1}) is assigned to charged Ru^{n+} carbonyl species and a lower energy region (2002–2099 cm^{-1}) can be ascribed to Ru^0 carbonyl clusters. In the case of Ru/HY, weak high energy bands are observed (2128, 2135, 2150, 2159 cm^{-1}). In the lower energy region, a strong band at 2099 and a triplet of medium bands (2028, 2048, 2080 cm^{-1}) are detected. The spectrum for Ru/NaY displays a high energy band at 2135 cm^{-1} and a triplet at 2002, 2033, and 2072 cm^{-1}. Fig. 4 shows the O–H region for Ru/HY prior to exposure to CO as spectrum A. Bands at 3743 (silanol), 3640 (supercage) and 3545 cm^{-1} (sodalite/hexagonal prism) are identified [8]. The intensity difference before and after exposure to CO is shown in fig. 4 as trace B. The finite difference could represent the amount of H^+ consumed in the supercage region.

Table 1
H/Ru ratios obtained from TPD data[a]

Sample	T_{red} (°C)	TPD (H/Ru)
Ru^N/NaY	500	0.57
Ru/NaY	500	0.55
	(autored. only)	0.41, 0.37 (2nd peak)
Ru/HY	500	0.14
	(autored. only)	0.21, 1.15 (2nd peak)

[a] 3 wt% metal loads; $T_{calc.}$ = 400°C.

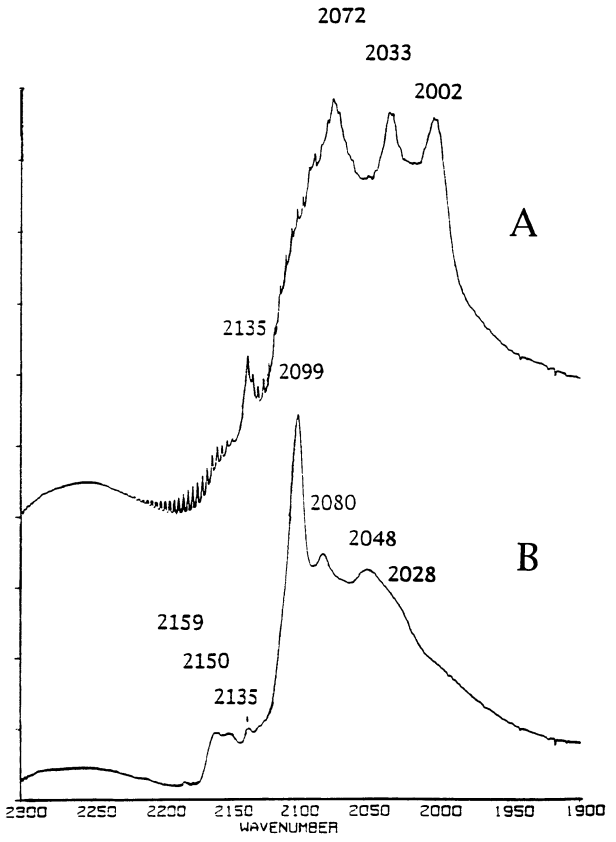

Fig. 3. FTIR spectra of the carbonyl region for: (A) Ru/NaY and (B) Ru/HY.

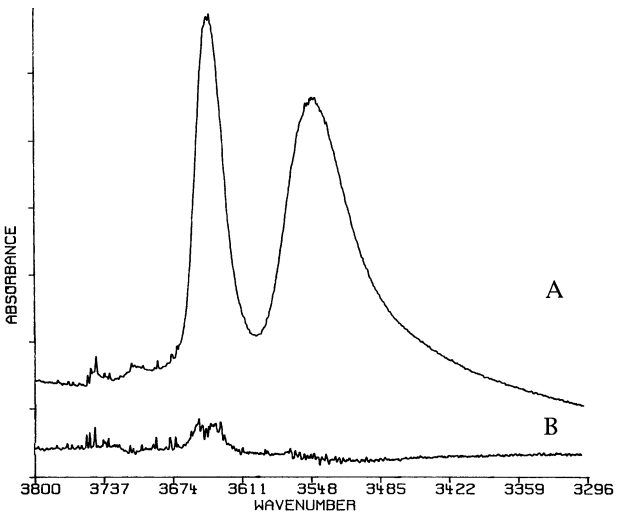

Fig. 4. (A) The O–H region for Ru/HY prior to exposure to CO. (B) Difference spectrum before and after exposure to CO.

The results for Ru/NaY are very similar to those obtained for Ru/HY.

3.4. TEM

Electron micrographs of Ru^N/NaY ($NaNO_3$) and Ru^N/NaY (NaOH) are shown in fig. 5. The samples were heated to 400°C under argon and reduced at 500°C. The electron micrograph of Ru^N/NaY ($NaNO_3$), shown in fig. 5a, is representative of the images found for Ru/NaY and Ru/HY. Analysis of the micrographs reveals similar particle sizes, based on the absence of any Ru metal particles larger than the zeolite Y supercage (13 Å), in Ru^N/NaY ($NaNO_3$), Ru/NaY, and Ru/HY. Treatment of Ru/NaY with NaOH to neutralize protons results in the formation of large particles (60–100 Å) after thermal treatment (fig. 5b). Several large particles were analyzed by EDS in order to confirm the presence of ruthenium.

3.5. EXAFS

The Fourier transforms of the k^3-weighted EXAFS oscillations $k^3\chi(k)$ of 3% Ru/NaY and 3% Ru/HY (heated to 400°C in helium and then subsequently reduced at 500°C) samples are shown in fig. 6 , traces A and B, respectively. A qualitative comparison of profiles A and B indicates that the coordination numbers of ruthenium for the two samples are similar. Fig. 7 shows a Ru/HY sample before (A) and after (B) reduction. The EXAFS parameters of all samples are shown in table 2.

4. Discussion

4.1. Effect of pretreatment conditions

Results by Goodwin et al. demonstrated that $[Ru(NH_3)_6]^{3+}$ ions in NaY cavities decompose under vacuum upon heating to 420°C to give very small Ru^0 clusters. EPR studies revealed no significant signal due to unreduced Ru^{n+} ($n = 1, 3, 5$) cations [9]. The present data are in agreement with these findings. Temperature-programmed mass-spectroscopic (TPMS) analysis reveals evolution of H_2, N_2 and NH_3 centered at $\sim$ 400°C indicating decomposition of $[Ru(NH_3)_6]^{3+}$/NaY upon heating in helium to 500°C (see fig. 1). Auto-reduction of ruthenium is complete, as further evidenced by the lack of H_2 consumption in the TPR profile to 650°C. Therefore, a pretreatment temperature of 400°C, with a heating rate of 2°C/min and an isotherm time of 20 min, was selected by previous authors [10] and in the present work, so as to obtain full decomposition of the ammine ligands. Our TEM data show that a low heating rate of 0.5°C/min to 400°C in helium leads to virtually the same metal particle size as heating with a 2°C/min ramp. The metal clusters formed in this way are very small, as evidenced by the extremely low Ru–Ru coordination numbers of 0.6 and 0.8 (table 2) and the invisibility of the clusters in TEM. They are smaller than the Y-supercages.

Subsequent treatment at 500°C in a hydrogen flow induces secondary agglomeration, as shown by the data

a

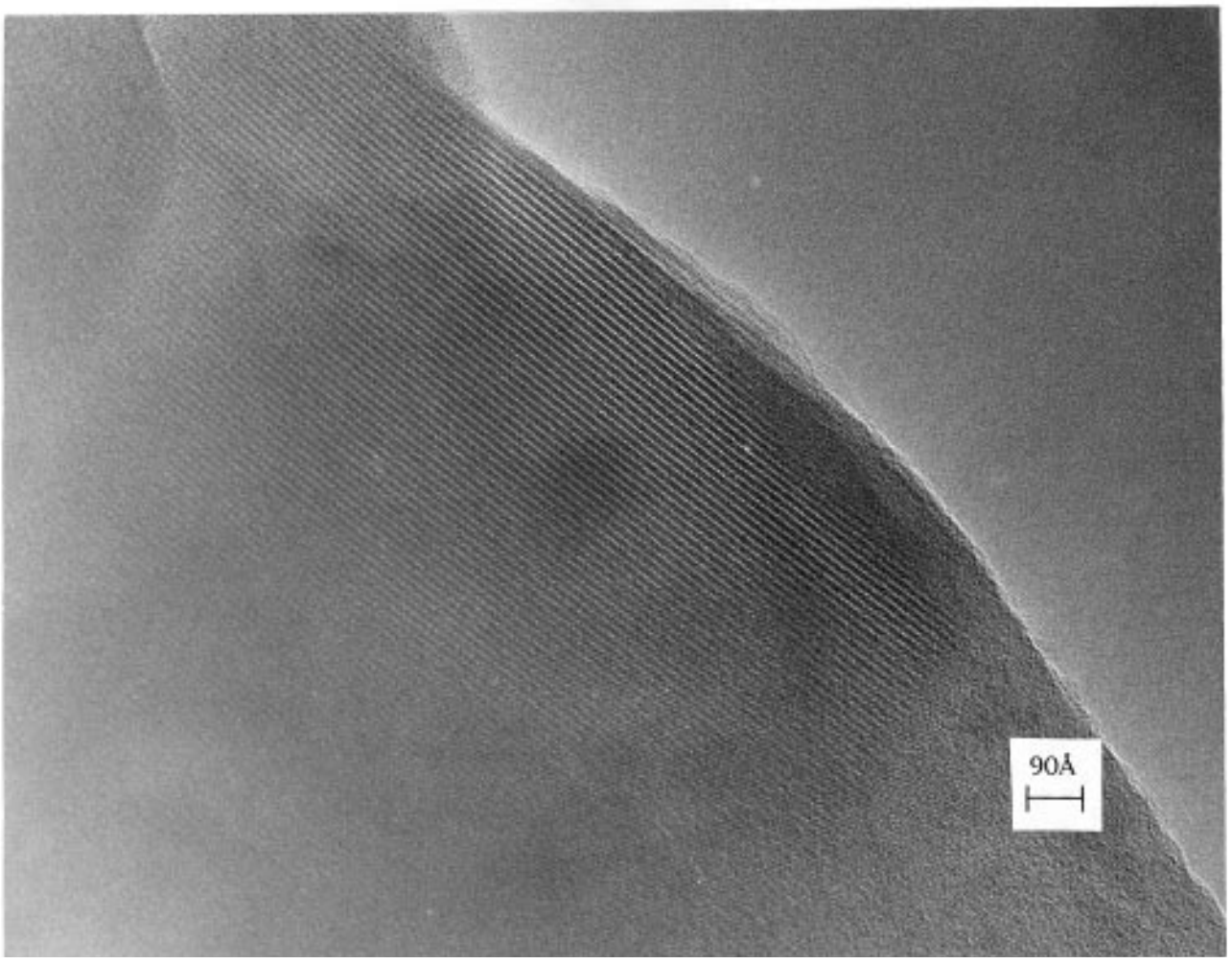

Fig. 5. TEM micrographs of samples after pretreatment in helium at 400°C and reduction at 500°C in H_2. (a) Ru^N/NaY ($NaNO_3$), magnification 150kx; (b) Ru^N/NaY (NaOH), magnification 400kx. (NB Figures are reduced to 75% of their original size.) (Continued on next page.)

in table 2 and in fig. 7 for Ru/HY. The Ru–Ru nearest neighbor interatomic distance was found to be smaller by as much as 0.08 Å (Ru/HY) than that in bulk Ru metal. Decreases in interatomic distances in small clusters have often been observed with small Ru particles [11,12] and those of other metals [13–16]. This bond length contraction is in agreement with quantum-chemical calculations performed on Ru_9 model clusters [17]. The peak at $\sim$ 1.86 Å in the Fourier transform without phase correction is shown in fig. 7b. The same distance was also observed in the Ru/Al_2O_3 system and was assigned to the interatomic distance between Ru^0 and the oxygen atoms of the support [11].

In the present work, the amount of hydrogen adsorption determined by TPD is crucial. In order to avoid uncertainties caused by hydrogen which might be desorbed only above 400°C, it was decided to focus on the secondary particles, formed at 500°C in flowing H_2. For brevity, the term "reduction" is used for the latter treatment although, strictly speaking, this term is correct only for the samples that were neutralized in air (see below), whereas all other primary particles had been chemically reduced in the preceding stage of autoreduction.

4.2. Neutralization of Ru/NaY

Reduction of Ru^{3+} ions to Ru^0 atoms produces three protons per Ru atom, notwithstanding whether the reduction is carried out by decomposing ammine ligands or in flowing H_2. Neutralization of the protons that were created during the reduction process was achieved in two ways: (1) "back-exchange" with an aqueous $NaNO_3$ solution; (2) washing with a NaOH solution (pH = 9.5). These methods resulted in very different Ru metal particle sizes. After pretreatment at 400°C in He and reduction to 500°C, the sample treated with NaOH gave *large* Ru metal particles (60–100 Å), whereas, the $NaNO_3$ back-exchanged sample gave small particles (10–15 Å) (see fig. 5). It is very likely that at a basic pH of 9.5, mobile ruthenium hydroxide species could agglomerate to form large particles. The reduction peak at 75°C for

b

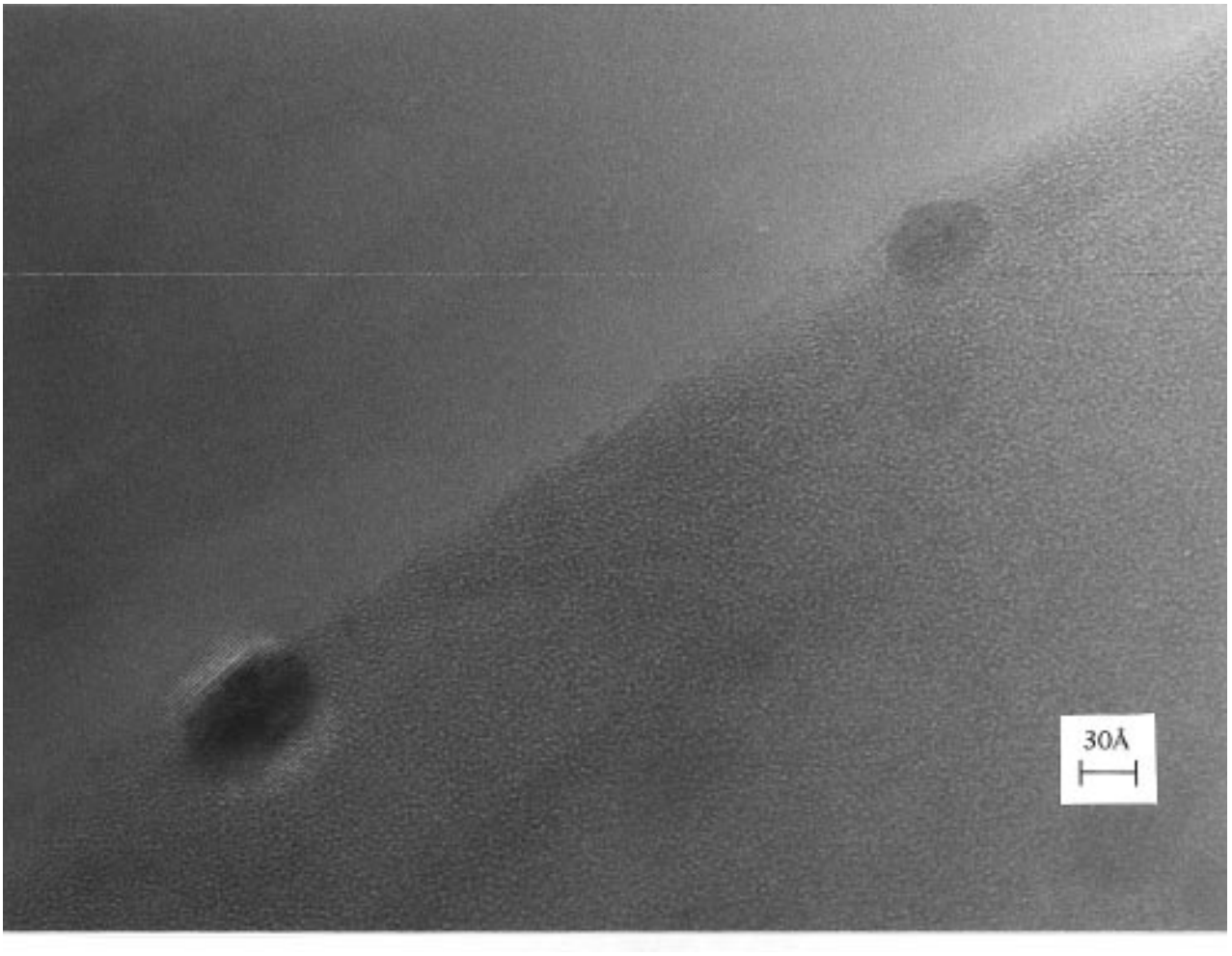

Fig. 5. (Continued.)

Ru^N/NaY ($NaNO_3$), shown in fig. 2, is assigned to ruthenium oxide. Since RuO_2 is the most stable oxide [18], the H/Ru ratio of 3.51 suggests that the interior of the ruthenium metal particles was not completely oxidized at room temperature during the exchange process. Kim et al. even detected by XPS a small amount of RuO_3 on the surface of RuO_2; so RuO_3 could also be present in our neutralized samples at room temperature [19].

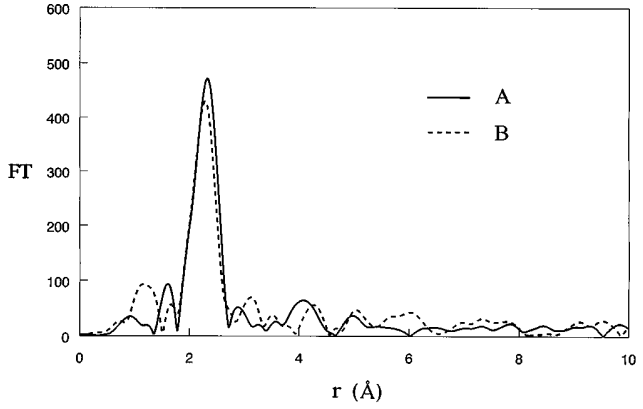

Fig. 6. EXAFS Fourier transforms for (a) Ru/NaY and (b) Ru/HY after pretreatment in helium at 400°C and reduction at 500°C.

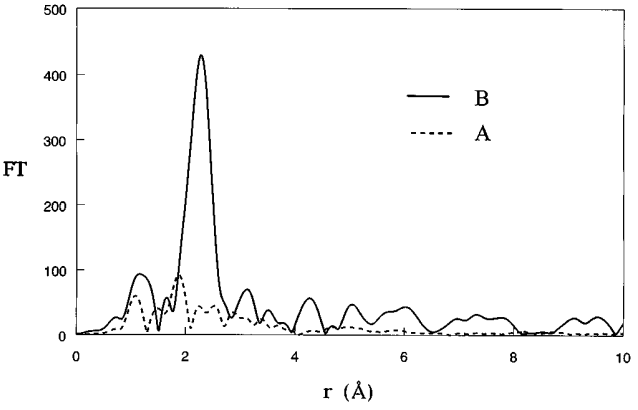

Fig. 7. EXAFS data for Ru/HY (a) prior to reduction and (b) after reduction at 500°C.

Table 2
EXAFS parameters of samples autoreduced at 400°C in helium, followed by treatment in flowing H_2 at T_{red} [a]

Sample [b]	T_{red} (°C)	CN	R (nm)
Ru^N/NaY	500	6.5	0.260
Ru/NaY	500	7.0	0.260
	(autored. only)	0.8	0.263
Ru/HY	500	6.2	0.259
	(autored. only)	0.6	0.261

[a] Notation: CN = coordination number; R = coordination distance.
[b] Metal loads of 3 wt%.

4.3. Suppression of hydrogen chemisorption

In the preceding section, samples had been compared which had either a small but finite (Ru/NaY), or a negligible (Ru^N/NaY) concentration of zeolite protons. In the present section, hydrogen adsorption is compared between samples of small (Ru/NaY) or very high (Ru/HY) proton concentration. Fortunately, the Ru/Y system permits us to address the fundamental question: which cause is responsible for the suppressed hydrogen adsorption? The Ru/Y system, unlike other M/Y systems, enabled us to synthesize samples with widely different proton concentrations but virtually equal metal particle sizes. As shown in table 2, Ru/NaY and Ru/HY have virtually identical metal particle sizes, but a pronounced suppression of the hydrogen chemisorption is observed for Ru/HY, whereas Ru/NaY has a much higher H_{ads}/Ru ratio (see table 1). It appears that the main cause of suppression of the hydrogen chemisorption is metal–proton interaction, not a reduction in metal particle size. The calculated proton/Ru ratio is 3 in the case of Ru/NaY after autoreduction. In this case the protons are a minority among the charge compensating cations; also the cages which hold Ru clusters will contain more Na^+ ions than protons. In contrast, all charge compensating ions are protons in Ru/HY and the proton/Ru ratio is 10.

The above results therefore suggest that proton-adduct formation leads to a change in the electronic structure of the Ru clusters and this induces a lowering of the propensity of these particles to chemisorb hydrogen. As this change in electronic structure has been described as *electron-deficiency* in the past [20–22], it is of interest to study these particles by infrared spectroscopy, using CO_{ads} as a probe molecule. Ru/NaY and Ru/HY have been selected for this comparison. Since Ru is one of the best catalysts for the hydrogenation of CO, there is extensive literature on the adsorption of CO on supported Ru and its FTIR spectroscopy [9,23–28]. The most prominent band in Ru/HY is located at 2099 cm^{-1} (see fig. 3B). Its intensity decreases as a function of purge time in He, while the triplet of bands at 2080, 2048 and 2028 cm^{-1} remains constant. This suggests that the high frequency band belongs to a different species than the triplet feature, although it might also reflect symmetry changes of a carbonyl cluster. Remarkably, this high frequency band is virtually absent in Ru/NaY. This leads to a tentative assignment of the 2099 cm^{-1} band to *a proton-anchored Ru–CO* complex. Analogous complexes have been identified in the Pd/zeolite Y system [26]. The shift of the C–O stretching frequency towards higher frequencies is consistent with less back-bonding and thus *electron-deficiency* of the Ru clusters in the Ru–proton adducts.

The aforementioned triplet could be ascribed to neutral $Ru_x(CO)_y$ clusters. Exchange of sodium ions by protons induces a blue shift of the carbonyl stretching frequencies ($2072 \rightarrow 2080$ cm^{-1}, $2033 \rightarrow 2048$ cm^{-1}, $2002 \rightarrow 2028$ cm^{-1}). This reflects a lower degree of back-bonding also from the metal to CO. These results suggest a transfer of electron density from the metal particles to the support, via an interaction between metal clusters and zeolitic protons. Similar effects have been observed in the Pd/zeolite Y system [29]. Since the shifts are relatively small and are complicated by dipole–dipole interactions, XPS experiments would help confirm this effect.

A cluster of bands between 2159 and 2135 cm^{-1} appears in Ru/HY and Ru/NaY. Their position is not sensitive to the nature of the cation (H^+ vs. Na^+). However, their stability upon He purge suggests a metal-bonded carbonyl. It is possible that these higher energy bands are due to $Ru^{n+}(CO)_2$ species. As shown in fig. 4, a small amount of H^+ is consumed in the supercage region. In a previous study of Rh/NaY, the supercage hydroxyl band was found to decrease upon CO admission to form $Rh^+(CO)_2$ [30]. Evolution of H_2 was confirmed with mass-spectrometric analysis. Similar chemistry has been suggested for the Ru/Al_2O_3 system, but no H_2 was detected after admission of CO [11].

Previously, it has been mentioned that the actual chemical nature of the H atoms for which we used the conventional term "zeolite protons" is possibly more similar to that of H atoms in "metal hydride" clusters, as described in the inorganic literature [31–34]. Each of these H atoms could cover more than one site, possibly adding a geometric cause to the observed suppression of H_2 chemisorption by "zeolite protons".

The present results suggest that the adsorption properties of small zeolite encaged metal clusters, and thus also their catalytic characteristics, can be "tuned" by interaction with other guest atoms or ions sharing the same zeolite cage.

5. Conclusion

A suppression of the propensity of small Ru clusters in Ru/HY to chemisorb hydrogen for Ru/HY has been observed. Comparison of samples with virtually equal Ru particle sizes, but markedly different proton concen-

trations, indicates that interaction of the metal clusters with zeolitic protons is the primary cause for this phenomenon. Infrared data are consistent with the model that Ru forms Ru–proton adducts in which the metal becomes *electron-deficient*. It stands to reason that the enthalpy of hydrogen chemisorption, ΔH_{ads}, is affected by this change in the electronic structure of the metal clusters and in addition by the geometric effect of the H atoms on the metal surface.

Acknowledgements

The authors gratefully acknowledge financial support from the National Science Foundation, Contract CTS-9221841. The ruthenium complex, $[Ru(NH_3)_6]Cl_3$, was obtained from Johnson/Matthey through their Precious Metals Loan Program. We wish to thank Dr. Ken Finkelstein, Cornell High Energy Synchrotron Source (CHESS), for assistance with EXAFS data collection and Professor Vinayak Dravid, Department of Materials Science, Northwestern University, for his permission to use the Hitachi HF-2000 electron microscope. We also wish to thank Dr. Tilman Beutel for helpful discussions.

References

[1] L. Xu, Z. Zhang and W.M.H. Sachtler, J. Chem. Soc. Faraday Trans. 88 (1992) 2291.
[2] D.C. Tomczak, G.-D. Lei, V. Schünemann, H. Treviño and W.M.H. Sachtler, Microporous Mater. 5 (1996) 263.
[3] P. Gallezot and B. Imelik, Adv. Chem. Ser. 121 (1973) 66.
[4] A.L. Yakovlev, G.M. Zhidomirov, K.M. Neyman, V.A. Nasluzov and N. Rösch, Ber. Bunsenges. Phys. Chem. 100 (1996) 1.
[5] A.L. Yakovlev, K.M. Neyman, G.M. Zhidomirov and N. Rösch, J. Phys. Chem. E, in press.
[6] H.T. Wang, Y.W. Chen and J.G. Goodwin Jr., Zeolites 4 (1984) 56.
[7] T.P. Kobylinski, B.W. Taylor and J. Young, Trans. Soc. Auto. Eng. 83 (1974) 1089.
[8] D.W. Breck, *Zeolite Molecular Sieves* (Wiley, New York, 1984).
[9] J.G. Goodwin Jr. and C. Naccache, J. Catal. 64 (1980) 482.
[10] L.A. Pederson and J.H. Lunsford, J. Catal. 61 (1980) 39.
[11] T. Mizushima, K. Tohji, Y. Udagawa and A. Ueno, J. Phys. Chem. 94 (1990) 4980.
[12] M.C.S. Sierra, J.G. Ruiz, M.G. Proietti and J. Blasco, J. Mol. Catal. A 96 (1995) 65.
[13] A. Balerna, E. Bernieri, P. Picozzi, A. Reale, S. Santucci, E. Burattini and S. Mobilio, Phys. Rev. B 31 (1985) 5058.
[14] P.A. Montano, W. Schulze, B. Tesche, G.K. Shenoy, T.I. Morrison, Phys. Rev. B 30 (1984) 672.
[15] B. Moraweck and A. Renouprez, J. Surf. Sci. 106 (1981) 35.
[16] G. Apai, J.F. Hamilton, J. Stohr and A. Thompson, Phys. Rev. Lett. 43 (1979) 165.
[17] A. Goursot, L. Pedocchi and B. Coq, J. Phys. Chem. 98 (1994) 8747.
[18] L. Brewer, Chem. Rev. 52 (1953) 1.
[19] K.S. Kim and N. Winograd, J. Catal. 35 (1974) 66.
[20] R.A. Della Betta and M. Boudart, in: *Proc. 5th Int. Congr. on Catalysis*, Palm Beach 1972, ed. H. Hightower (North-Holland, Amsterdam, 1973) p. 1329.
[21] X.L. Bai and W.M.H. Sachtler, J. Catal. 129 (1991) 121.
[22] W.M.H. Sachtler and A.Y. Stakheev, Catal. Today 12 (1992) 283.
[23] A. Zecchina and E. Guglielminotti, J. Catal. 74 (1982) 225.
[24] S. Uchiyama and B.C. Gates, J. Catal. 110 (1988) 338.
[25] F. Solymosi and J. Raskó, J. Catal. 115 (1989) 107.
[26] V.L. Kuznetsov, A.T. Bell and Y. Yermakov, J. Catal. 65 (1980) 374.
[27] R.A. Dalla Betta, J. Phys. Chem. 79 (1975) 2519.
[28] H. Chen, Z. Zhong and J.M. White, J. Catal. 90 (1984) 119.
[29] L.L. Sheu, H. Knözinger and W.M.H. Sachtler, J. Am. Chem. Soc. 111 (1989) 8125.
[30] T.T.T. Wong, A.Y. Stakheev and W.M.H. Sachtler, J. Phys. Chem. 96 (1992) 1733.
[31] W.M.H. Sachtler, in: *Handbook of Catalysis*, eds. G. Ertl, H. Knözinger and J. Weitkamp (Verlag Chemie, Weinheim) ch. 1.2.3.4, in press.
[32] S.G. Kazarian, P.A. Hamley, M. Poliakof, J. Am. Chem. Soc. 115 (1993) 9069.
[33] I.C.M. Wehman-Ooyevaar, D.M. Grove, P. de Vaal, A. Dedieu, G. van Koten, Inorg. Chem. 31 (1992) 5484.
[34] I.C.M. Wehman-Ooyevaar, D.M. Grove, H. Kooijman, P. van der Sluis, A.L. Spek and G. van Koten, J. Am. Chem. Soc. 114 (1992) 9916.